Power Electronic Systems
Laboratory

© 2020 IEEE

IEEE Transactions on Biomedical Engineering (Early Access)

CFD Assisted Evaluation of In Vitro Experiments on Bearingless Blood Pumps

P. Puentener,
M. Schuck,
J. W. Kolar

Personal use of this material is permitted. Permission from IEEE must be obtained for all other uses, in any current or future media, including reprinting/republishing this material for advertising or promotional purposes, creating new collective works, for resale or redistribution to servers or lists, or reuse of any copyrighted component of this work in other works.

Eidgenössische Technische Hochschule Zürich
Swiss Federal Institute of Technology Zurich

This article has been accepted for publication in a future issue of this journal, but has not been fully edited. Content may change prior to final publication. Citation information: DOI 10.1109/TBME.2020.3030316, IEEE Transactions on Biomedical Engineering

CFD Assisted Evaluation of in Vitro Experiments on Bearingless Blood Pumps

Pascal Puentener, *Student Member, IEEE* , Marcel Schuck, *Member, IEEE* and Johann W. Kolar, *Fellow, IEEE*

***Abstract*— *Objective:* This paper presents a comparative study of computational fluid dynamic (CFD) simulations and in vitro hemolysis examinations of a bearingless centrifugal blood pump. The outcomes of the in vitro study are analyzed with the help of CFD hemolysis models. *Methods:* Several pump prototypes were manufactured and tested. Each model was implemented in a CFD framework and simulated with different Eulerian hemolysis models. The outcomes are compared to experimental data. The model achieving the highest correlation is used to explain the in vitro outcomes in detail. *Results:* It is shown that a double-stage model achieves the best correlation. The sensitivity of the simulation is considerably lower than that of in vitro tests. The CFD model reveals that most of the cell destruction is caused in the radial gap of the pump. Further critical regions are the bottom volume and the shroud clearance gap. Only 0.5% of the priming volume is subject to overcritical shear stress. *Conclusion:* Cell compatibility can be improved by increasing the radial gap, lowering the shroud and hub clearance gaps, and increasing the fillet radius of the inlet nozzle. CFD models can be used to examine the cell damage effects and help to further improve the pump design. *Significance:* This paper compares different Eulerian CFD hemolysis models, parameter sets, and equivalent shear stresses to several in vitro hemolysis tests. The sensitivity of the models is compared to that of in vitro studies. It is shown that CFD simulations have their limitations but can help with interpreting the outcomes of in vitro studies.**

***Index Terms*— bearingless, blood damage, centrifugal pumps, extracorporeal life support, hemolysis, in vitro, magnetic levitation, CFD simulation.**

I. Introduction

Mechanical life support procedures require specialized blood pumps to maintain blood flow during heart insufficiency or failure. To date, most of the used devices are centrifugal pumps [1]. However, the use of these devices can cause severe complications, such as bleeding, thrombus formation or hemolysis. Due to the excessive shear stress inside the pump, the membrane of the red blood cells (RBC) can get damaged, leading to a dysfunction. This can cause renal and multi-organ failure [2], [3]. To improve the outcome of mechanical life support treatments, it is important to reduce the cell damage within these pumps.

In recent years, the use of computational fluid dynamics (CFD) simulations to predict the cell damage has become an important design tool for developing novel blood pumps [4]–[6]. Due to the lack of an universally applicable, reliable model, such simulations often overestimate the cell damage and do not provide reliable predictions [7], [8]. Still, they provide important insight into the damage mechanism within the pump and can help to identify critical locations.

In this study, the correlation between different hemolysis models and in vitro experiments is analyzed for geometric variations of the pump head. The best suited model is then used to explain the outcomes of the in vitro experiments conducted with the pump prototypes.

II. Hemolysis Models

The destruction of a RBC causes its contained hemoglobin (Hb) to be released into the blood plasma. The amount of cell damage can be expressed by the amount of plasma-free hemoglobin (pfHb). For CFD simulations it is common to use the so-called index of hemolysis

$$\mathrm{HI} = \frac{\Delta \mathrm{pfHb}}{\mathrm{Hb}}. \tag{1}$$

A mathematical model to estimate the shear induced hemolysis was derived by Giersiepen, based on experimental data of Wurzinger [9], [10]. The so-called power law model

$$\mathrm{HI} = c_{\mathrm{hem}} t_{\mathrm{exp}}^{\alpha} \tau^{\beta} \tag{2}$$

connects the two main influencing factors, namely the scalar shear stress τ and exposure time t_{exp}, to the hemolysis index.

The exponent $\alpha < 1$ can be explained by a hardening of the RBC membrane under shear stress [11].

Several authors conducted experiments to find a threshold level above which hemolysis occurs [12]–[20]. It was found that this threshold τ_{S} is time dependent and can be written as [21], [22]

$$\tau_{\mathrm{S}} = 88.905 \cdot t_{\mathrm{exp}}^{-0.3372}. \tag{3}$$

This work was supported by the Swiss Commission for Technology and Innovation CTI-KTI.

Pascal Puentener (puentener@lem.ee.ethz.ch), Marcel Schuck (schuck@lem.ee.ethz.ch) and Johann W. Kolar (kolar@lem.ee.ethz.ch) are with the Power Electronic Systems Laboratory, ETH Zurich, Switzerland.

Corresponding author: Marcel Schuck, Power Electronic Systems Laboratory, ETH Zurich, Physikstrasse 3, 8092 Zurich, Switzerland.
e-mail: schuck@lem.ee.ethz.ch

Copyright (c) 2020 IEEE. Personal use of this material is permitted. However, permission to use this material for any other purposes must be obtained from the IEEE by sending an email to pubs-permissions@ieee.org.

0018-9294 (c) 2020 IEEE. Personal use is permitted, but republication/redistribution requires IEEE permission. See http://www.ieee.org/publications_standards/publications/rights/index.html for more information.
Authorized licensed use limited to: ETH BIBLIOTHEK ZURICH. Downloaded on October 15,2020 at 12:50:59 UTC from IEEE Xplore. Restrictions apply.

This article has been accepted for publication in a future issue of this journal, but has not been fully edited. Content may change prior to final publication. Citation information: DOI 10.1109/TBME.2020.3030316, IEEE Transactions on Biomedical Engineering

Based on this knowledge, several hemolysis models were derived and implemented in CFD simulations. Common approaches use a Lagrangian formulation, calculating the amount of hemolysis in a post-processing stage by means of particle tracking. The flow field is obtained by solving the Navier-Stokes equations independently of the hemolysis models, which makes this approach computationally attractive. The drawback is that only a finite number of particles can be seeded. The amount of hemolysis captured by the particles depends on their trajectory and, thus, on the initial seeding position.

Alternative approaches use an Eulerian formulation. The hemolysis models are first reformulated to be linear in time and then implemented in the CFD solver as an additional transport equation. Such models require more computational power but provide a scalar field of the hemolysis index. Thus, critical regions can be identified better and the results are not affected by any user-dependent post-processing.

Unfortunately, no common agreement about the way to implement such Eulerian models exits, nor what parameters and equivalent shear stress to use. Only few researchers compared their results to in vitro experiments. While some conclude that the reliability of the models is insufficient [8], [23], others find good agreement and correlation to in vitro tests [24]–[26]. To the authors knowledge, a sensitivity analysis of different models with in vitro experiments was not carried out so far.

A. Implementations

For the Eulerian approach, several implementation methods were suggested. In the following, two of them are presented.

1) Single-Stage Model

The first Eulerian implementation of the power law model was presented in 2007. Due to the nonlinear relation between exposure time and hemolysis, this model cannot be easily implemented in regular CFD solvers. To overcome this issue, equation (2) must be scaled to obtain a linear relation [27].

This can be done by introducing an additional variable HL subject to

$$\mathrm{HI} = \mathrm{HL}^{\alpha}, \tag{4}$$

leading to the power law

$$\mathrm{HL}^{\alpha} = \left[(c_{\mathrm{hem}} \tau^{\beta})^{1/\alpha} t \right]^{\alpha}. \tag{5}$$

Since the term in square brackets is linear in time, it can be implemented as a source term S_{HL} of the transport equation

$$\frac{\partial \mathrm{HL}}{\partial t} + (\vec{v} \cdot \nabla)\mathrm{HL} = S_{\mathrm{HL}} \tag{6}$$

$$S_{\mathrm{HL}} = (c_{\mathrm{hem}} \tau^{\beta})^{1/\alpha}, \tag{7}$$

where $\vec{v}$ is the velocity field. The variable HL can be calculated using a CFD solver. The hemolysis index HI is then obtained from equation (4).

Even though the initial power law of equation (2) is time dependent, the single-stage implementation ignores the load history of the cell. At any point in time, the amount of generated hemolysis only depends on the source term S_{HL}. Thus, it is directly related to the local shear stress τ. Still, this model is frequently used and discussed [7], [23], [27]–[29].

2) Double-Stage Models

Instead of directly relating hemolysis to the local shear stress, alternative implementations, that are capable of capturing the membrane hardening, can be obtained by solving an additional transport equation [30]

$$\frac{\partial \psi}{\partial t} + (\vec{v} \cdot \nabla)\, \psi = 1 \qquad \text{or} \tag{8}$$

$$\frac{\partial D_{\mathrm{b}}}{\partial t} + (\vec{v} \cdot \nabla)\, D_{\mathrm{b}} = \tau^{\beta/\alpha}. \tag{9}$$

These two transport equations accumulate the residence time ψ or damage dose D_{b} of the RBC, respectively, along the trajectories of particles. Therefore, they contain information about the history of the cell.

The locally generated hemolysis, S_{HI}, can then be weighted by these two quantities. This results in the hemolysis transport equation

$$\frac{\partial \mathrm{HI}}{\partial t} + (\vec{v} \cdot \nabla)\, \mathrm{HI} = S_{\mathrm{HI}}, \tag{10}$$

with the respective source term

$$S_{\mathrm{HI},\Psi} = \alpha c_{\mathrm{hem}} \psi^{\alpha-1} \tau^{\beta} \quad \text{or} \tag{11}$$

$$S_{\mathrm{HI},\mathrm{D_b}} = \alpha c_{\mathrm{hem}} D_{\mathrm{b}}^{\alpha-1} \tau^{\beta/\alpha}. \tag{12}$$

In contrast to the single-stage model, membrane hardening is considered. The additional transport equation, however, increases the required computational power. Additional thresholds of the shear stress can be implemented by weighting the hemolysis transport equations.

III. Parameters and Equivalent Shear

The parameter set obtained by Giersiepen (equation (2)) is known to overestimate hemolysis by more than one magnitude [22]. In [31] an overestimation by three magnitudes was reported. To achieve better agreement with measurements, several authors have introduced additional parameter sets, which are listed in Table I. Their validity range remains mostly unclear and no universally applicable formulation has been given so far [7]. Parameter sets evaluated in this work are marked with an asterisk.

TABLE I
PARAMETER SETS RECOMMENDED OR USED BY DIFFERENT AUTHORS.

c_{hem}	α	β	Author
$1.210 \cdot 10^{-7}$	0.7470	2.0040	Taskin [32]
$3.620 \cdot 10^{-7}$	0.7850	2.4160	Giersiepen* [9], [33], [34]
$1.508 \cdot 10^{-8}$	0.7850	2.4160	Goubergrits* [22]
$1.800 \cdot 10^{-8}$	0.7650	1.9910	Heuser* [16], [35]
$1.228 \cdot 10^{-7}$	0.6606	1.9918	Zhang [36]
$1.745 \cdot 10^{-8}$	0.7762	1.963	Fraser* [37]

In addition, it remains unclear how to represent the three-dimensional stress tensor $\underline{\tau}$ by a scalar equivalent stress τ. Most formulations use a combination of the first and second main invariant of the stress tensor $\underline{\tau}$

$$I_{\tau} = \mathrm{tr}(\underline{\tau}) \qquad \text{and} \tag{13}$$

$$II_{\tau} = \frac{1}{2}\left(\mathrm{tr}(\underline{\tau})^2 - \mathrm{tr}(\underline{\tau}^2)\right). \tag{14}$$

0018-9294 (c) 2020 IEEE. Personal use is permitted, but republication/redistribution requires IEEE permission. See http://www.ieee.org/publications_standards/publications/rights/index.html for more information.
Authorized licensed use limited to: ETH BIBLIOTHEK ZURICH. Downloaded on October 15,2020 at 12:50:59 UTC from IEEE Xplore. Restrictions apply.

This article has been accepted for publication in a future issue of this journal, but has not been fully edited. Content may change prior to final publication. Citation information: DOI 10.1109/TBME.2020.3030316, IEEE Transactions on Biomedical Engineering

A list of possible implementations is given in Table II.

TABLE II
POSSIBLE SCALAR EQUIVALENT SHEAR STRESS FORMULATIONS.

Variable	Relation to $\underline{\tau}$	Authors
τ_{vM}	$\sqrt{\frac{3}{2}(I_\tau^2 - 2II_\tau)}$	[38]
$\tau^*_{\sqrt{3}}$	$\sqrt{\frac{1}{2}(I_\tau^2 - 2II_\tau)}$	[34], [39], [40]
τ_{II}	$\sqrt{-nII_\tau}, \quad n = 1, 2, 3...$	[7]
τ^*_{B}	$\sqrt{\frac{1}{6}\sum_{i\neq j}(\tau_{ii} - \tau_{jj})^2 + \sum_{i\neq j}\tau_{ij}^2}$	[41]
τ_{Y}	$\sqrt{\sum_{i\neq j}(\tau_{ii} - \tau_{jj})^2 + \sum_{i\neq j}\tau_{ij}^2}$	[7]

IV. In vitro Experiments

To evaluate the reliability of the different hemolysis models with respect to geometry variations on the pump, experiments with nine variations of a magnetically levitated centrifugal pump were conducted. For each of these, prototypes were simulated, manufactured, and tested in an in vitro study. The results of the experimental and simulative studies were then compared to each other. In the following, the examined pump prototypes, the in vitro experiments, and the implementation of the CFD studies are described in more detail.

A. Pump Design and Variations

As a base design, a bearingless centrifugal pump was designed for a nominal pressure difference of $350\,\mathrm{mmHg}$ at a flow rate of $5\,\mathrm{l/min}$, using semi-empirical formulas according to Gülich [42]. The resulting design has an impeller diameter of $22\,\mathrm{mm}$, blade height of $6\,\mathrm{mm}$, blade angle of $90°$, and is operated at a nominal rotational speed of $7885\,\mathrm{rpm}$.

This design, together with cut-views of the impeller, is shown in Fig. 1. Since the design of impeller SO with extended blades deviates from the base design, a photograph is added on the left hand side. This impeller is designed to minimize the relative speed within the radial fuild gap between the impeller and the housing.

Nine variations of the base design were tested, each varying in a single dimension. A list of the variations is given in Table III.

B. Test Setup

The prototypes were tested at the nominal operating point in an in vitro test bench as schematically shown in Fig. 2, using bovine blood according to the ASTM Standard [43]. Blood was collected from a local slaughterhouse, drained directly after the neck cut, mixed with $8000\,\mathrm{IU/l}$ heparin anticoagulant, and transported to the laboratory in a closed container. The blood was then filtered and diluted to a hematocrit (Hct) of 30% using phosphate buffered saline (PBS). Between collection of the blood and the start of the experiment, no more than 1 hour elapsed. Any equipment getting in contact with the blood was first rinsed with PBS.

The experiments were conducted for 6 hours. Samples were taken at a regular time interval of 1 hour. The blood was tempered to $30\,°\mathrm{C}$.

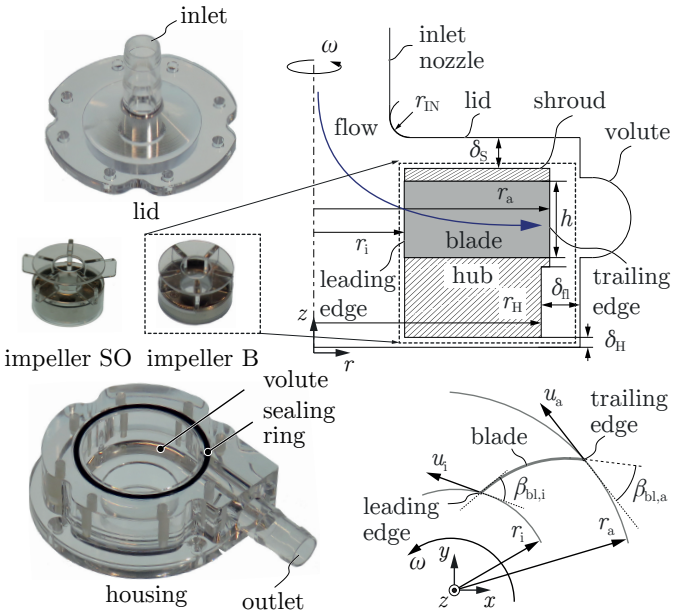

Fig. 1. Photograph of the base design pumphead prototype milled from polycarbonate.

TABLE III
LIST OF TESTED IMPELLER VARIATIONS, ROTATIONAL SPEED n AND HEMOLYSIS RESULTS.

Design	Varied	Change	n/rpm	RIH	$\mathrm{RIH/RIH_B}$
B	-	-	7885	0.625	1
B+	h	$+1\,\mathrm{mm}$	7775	0.605	0.968
B-	h	$-1\,\mathrm{mm}$	8055	0.948	1.5168
RG+	δ_{fl}	$+0.5\,\mathrm{mm}$	7825	0.458	0.7328
D-	r_{a}, r_{H}	$-0.5\,\mathrm{mm}$	8270	0.500	0.8
SO	r_{a}	$+4\,\mathrm{mm}$	5635	0.933	1.4928
A60	$\beta_{\mathrm{bl,a}}$	$-30°$	8055	0.978	1.5648
H-	δ_{H}	$-2\,\mathrm{mm}$	7915	0.541	0.866
S+	δ_{S}	$+2\,\mathrm{mm}$	7950	1.288	2.061
R+	r_{IN}	$+5\,\mathrm{mm}$	7845	0.387	0.619

The amount of pfHb was identified by a Drabkin's assay measuring the absorbance of plasma at a wavelength of $540\,\mathrm{nm}$ [44]. Finally, the normalized index of hemolysis (NIH) was calculated according to

$$\mathrm{NIH} = \frac{\Delta\mathrm{pfHb}}{\Delta t} \cdot \frac{V}{Q}(1 - \mathrm{Hct}), \tag{15}$$

where, Q and V represent the flow rate and circuit volume, respectively. The rate of pfHb over time was obtained by a linear regression.

The measured NIH and the HI used in the CFD models are related by

$$\mathrm{HI} = \frac{\mathrm{NIH}}{\mathrm{Hb}} \cdot \frac{1}{1 - \mathrm{Hct}}. \tag{16}$$

This represents the amount of hemoglobin Hb released into the plasma for a single pass through the pump.

C. Reference Pump

To reduce the effect of the variation of the blood across different tests, a commercial centrifugal pump was run in

0018-9294 (c) 2020 IEEE. Personal use is permitted, but republication/redistribution requires IEEE permission. See http://www.ieee.org/publications_standards/publications/rights/index.html for more information.
Authorized licensed use limited to: ETH BIBLIOTHEK ZURICH. Downloaded on October 15,2020 at 12:50:59 UTC from IEEE Xplore. Restrictions apply.

This article has been accepted for publication in a future issue of this journal, but has not been fully edited. Content may change prior to final publication. Citation information: DOI 10.1109/TBME.2020.3030316, IEEE Transactions on Biomedical Engineering

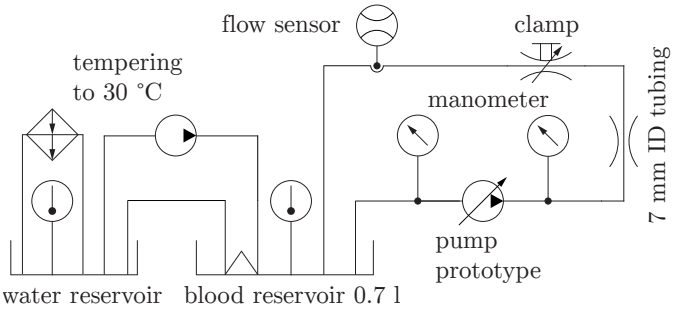

Fig. 2. Schematic drawing of the in vitro test bench used to evaluate the hemolysis generation of the prototypes.

parallel for each test. This pump acted as a reference, providing a reference NIH ($\mathrm{NIH_{ref}}$). With this, a relative NIH $\mathrm{RIH} = \mathrm{NIH}/\mathrm{NIH_{ref}}$ is calculated for every prototype. These RIH values can be used to compare the relative increase or reduction in hemolysis between the prototype pumps across different tests.

D. In Vitro Results

The base design pump was tested $N = 16$ times, showing an average hemolysis of $\mathrm{NIH} = 0.0096\,\mathrm{mg/dl}$. This is 5 times lower than the additionally tested Medtronic BPX-80 pump ($N = 14$, $\mathrm{NIH} = 0.0502\,\mathrm{mg/dl}$, $p < 0.001$). The prototypes thus generate as little damage as commercial centrifugal pumps for medical applications [45], [46].

A summary of the test results is given in Table III. The $\mathrm{RIH}/\mathrm{RIH_B}$ relates the variations to the base design B.

Comparing the $\mathrm{RIH}/\mathrm{RIH_B}$ reveals that increasing the radial gap (design RG+ and D-) leads to a reduction of hemolysis. Increasing the blade height (B+) results in almost no change. Further improvement can be achieved with a rounded inlet nozzle (R+) and lower hub clearance gap (H-). Other designs lead to an increased cell damage. These include a reduced blade height (B-), extended blade length (SO), an increased shroud clearance gap (S+) and 60° blade angle (A60).

V. CFD Implementations

The various prototypes were implemented in ANSYS CFX together with the hemolysis models described above. The impeller speed was set to the nominal speed listed in Table III.

Diffusion of hemolysis was neglected as the residence time within the pump volume is short at a flow rate of $5\,\mathrm{l/min}$.

Blood was modeled as a Newtonian fluid with a viscosity of $3.5\,\mathrm{mPa \cdot s}$ and a density of $1060\,\mathrm{kg/m^3}$. This is a reasonable assumption for the shear strains present in centrifugal pumps [6]. Turbulence was modeled by the Reynolds-averaged Navier-Stokes equations with a $k-\omega$ SST model [47].

At the boundary of the inlet, the total mass flow was specified whereas at the outlet a static pressure boundary condition was defined.

It should be noted that a small ($< 1\,\mathrm{mm}$) time-variant axial displacement of the impeller occurs in a practical pump during operation. Due to the stochastic nature of these movements, this effect cannot be simulated appropriately.

A. Mesh Independence Study

In a first step, a mesh independence study was conducted on the base design B at its nominal operating point. The simulation results for the pressure difference Δp and hemolysis HI for mesh sizes of 2 to 8 million (m) cells were compared to a model with 15m cells. The resolution of the boundary layer was fixed during variation.

The percentage differences to this model are shown in Fig. 3.

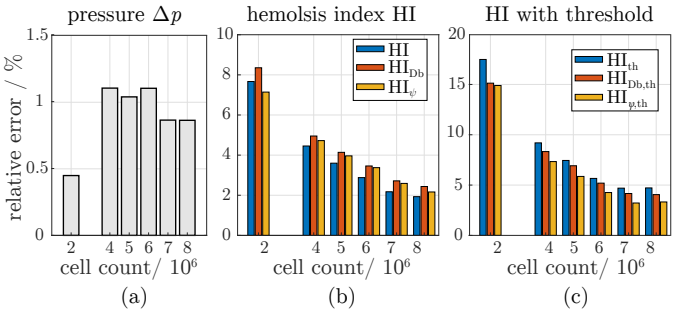

Fig. 3. Relative error of the simulated pressure difference $\boldsymbol{\Delta p}$ (a) and hemolysis index $\mathbf{HI}$ (b & c) of the base design B as a function of the cell count compared to a model with 15 million cells.

Pressure predictions are almost independent of the mesh size above 4m cells. The difference between 8m and 15m cells is below 1%. Mesh independence of the hemolysis models is obtained at higher cell counts. The difference between 8m and 15m is around 2% for models without shear stress threshold, and around 5% if a threshold of $\tau_S = 150\,\mathrm{Pa}$ is implemented. A final mesh with 8m cells was used, resulting in an error of the pressure difference of less than 10% compared to measurements.

B. Boundary Layer

To resolve the boundary layer profile, 15 inflation layers were introduced on all surfaces with a height of the first cell of $5\,\mu\mathrm{m}$. This ensures that the y^+ value is close to one and the viscous sublayer is resolved. Fig. 4 shows the distribution of the first cell layer along the dimensionless wall distance y^+ and the velocity profile of the turbulent boundary layer according to [48]. Further mesh refinements to $y^+ = 0.1$ improves the resolution of the maximum shear stress [49] but results in a significantly higher number of mesh elements and considerably longer computational times, for which design variations become impractical.

C. Convergence

To achieve fast convergence, all CFD models were first simulated using a frozen rotor interface. With this, only the flow field was solved without any hemolysis model implemented. After 1000 iterations, the residuals reduced to approximately 10^{-3}_{rms} and the pressure difference across the pump settled to a steady value. Using this flow field, another frozen rotor simulation was initialized additionally solving for the hemolysis transport equations. After approximately 2000 iterations, the hemolysis at the pump outlet settles. The hemolysis models

0018-9294 (c) 2020 IEEE. Personal use is permitted, but republication/redistribution requires IEEE permission. See http://www.ieee.org/publications_standards/publications/rights/index.html for more information.
Authorized licensed use limited to: ETH BIBLIOTHEK ZURICH. Downloaded on October 15,2020 at 12:50:59 UTC from IEEE Xplore. Restrictions apply.

This article has been accepted for publication in a future issue of this journal, but has not been fully edited. Content may change prior to final publication. Citation information: DOI 10.1109/TBME.2020.3030316, IEEE Transactions on Biomedical Engineering

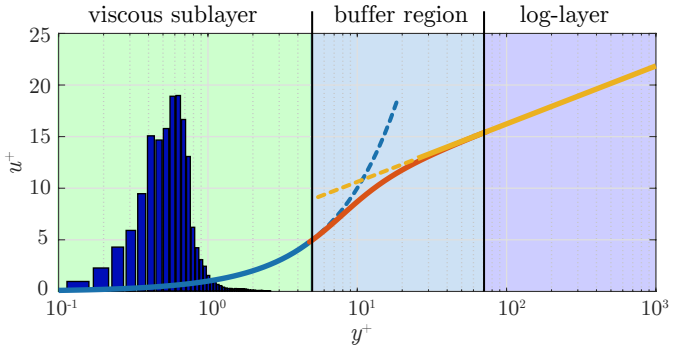

Fig. 4. y^+ distribution of the implemented CFD model. The target was to achieve $y^+_{\mathbf{mean}} \approx \mathbf{1}$.

are assumed to be converged when the mass flow averaged hemolysis index at the outlet

$$\mathrm{HI}_{\mathrm{CFD}}(t) = \frac{\int_{\partial A} \mathrm{HI}\dot{m}\,\mathrm{d}A}{\int_{\partial A} \dot{m}\,\mathrm{d}A}, \tag{17}$$

does not change more than 1% across the last 100 iterations.

With this result, transient simulations of the impeller were initialized and simulated using a time-step size of $0.1/\omega$, where ω is the rotational speed of the impeller, for an additional 5 impeller rotations. For the transient simulations maximum residuals of 10^{-4} were targeted and the chosen time-step size resulted in good conversion properties. Mass and momentum residuals reduced to $< 10^{-5}$ and $< 5 \cdot 10^{-5}$, respectively. Domain imbalances were below 0.1%.

D. Parameter Choice

To obtain the best combination of parameter set and equivalent shear stress, the parameter sets of Fraser (FR), Heuser (HE), Goubergrits (GG) and Giersiepen (GS) as well as the two scalar shear stresses $\tau_{\sqrt{3}}$ and τ_{B} were implemented in a frozen-rotor simulation and compared to in vitro hemolysis results. The relative error of the different combinations is listed in Table IV.

While the parameter set GS with the equivalent stress fomulation τ_{B} results in an overestimation of the cell destruction by 6300%, better agreement can be achieved with the parameter set FR and an equivalent shear stress $\tau_{\sqrt{3}}$. This combination still overestimates the hemolysis by 197%.

TABLE IV
RELATIVE ERROR OF SIMULATIONS TO MEASUREMENTS CAUSED BY PARAMETER CHOICE.

relative error	parameter set FR	HE	GG	GS
τ_{B}	2.3	3.1	25.4	633.4
$\tau_{\sqrt{3}}$	2.0	2.7	22.7	569.0

E. Implementation Method

To choose the best implementation method, the single-stage and double-stage models were implemented, both, with and without threshold levels.

According to equation (3), the expected threshold level for an average residence time of $t_{\mathrm{exp}} = V/Q \approx 200\,\mathrm{ms}$ is close to $\tau_{\mathrm{S}} = 150\,\mathrm{Pa}$. This is also the value recommended and used by [6], [50], [51]. In the present work, the threshold was implemented by weighting the hemolysis source term by

$$w(\tau) = \frac{1}{2}\left(\tanh\left(5\frac{\tau - \tau_{\mathrm{S}}}{\tau_{\mathrm{S}}}\right) + 1\right). \tag{18}$$

A schematic illustration of the different implemented hemolysis models is illustrated in Fig. 5.

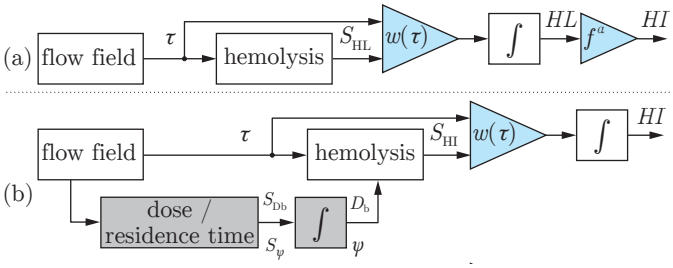

Fig. 5. Flow charts of the implemented hemolysis models, corresponding to equations (4)-(6) (a), and equations (8) - (12) (b).

The relative error of the hemolysis prediction compared to in vitro experiments is listed in Table V. Best agreement is achieved by the double-stage model with a residence time source term (DSR). Its relative error is 9%.

TABLE V
RELATIVE MODEL ERROR OF SIMULATIONS TO MEASUREMENTS BY IMPLEMENTATION METHOD.

implementation	equations	HI / 10^{-6}	e_{rel} / %
in vitro	(16)	1.37	0
single-stage (SS)	(6)	4.08	+197
double-stage dose (DSD)	(12)	2.63	+92
double-stage time (DSR)	(11)	1.49	+9
SS with τ_{th}	(6)+(18)	2.23	+63
DSD with τ_{th}	(12)+(18)	1.12	-18
DSR with τ_{th}	(12)+(18)	4.76	-65

F. Sensitivity Analysis

To evaluate the sensitivity of the simulations, the RIH of the CFD simulations is compared to the mean RIH of the in vitro experiments.

Results for various implementations are shown in Fig. 6. The in vitro test results are listed on the far left, sorted by increasing RIH. For each experiment, the p-value of a two-sided t-test, comparing the respective result to the base design B (white bar), is listed above the respective bar.

Highest correlation is achieved by the DSR model (correlation coefficient 0.84). Still, the sensitivity is much lower than for in vitro experiments. Especially, the impeller design A60 tends to perform better than the base design B according to CFD simulations. At the same time, this impeller caused significantly more cell damage than the base design B during in vitro tests.

0018-9294 (c) 2020 IEEE. Personal use is permitted, but republication/redistribution requires IEEE permission. See http://www.ieee.org/publications_standards/publications/rights/index.html for more information.
Authorized licensed use limited to: ETH BIBLIOTHEK ZURICH. Downloaded on October 15,2020 at 12:50:59 UTC from IEEE Xplore. Restrictions apply.

This article has been accepted for publication in a future issue of this journal, but has not been fully edited. Content may change prior to final publication. Citation information: DOI 10.1109/TBME.2020.3030316, IEEE Transactions on Biomedical Engineering

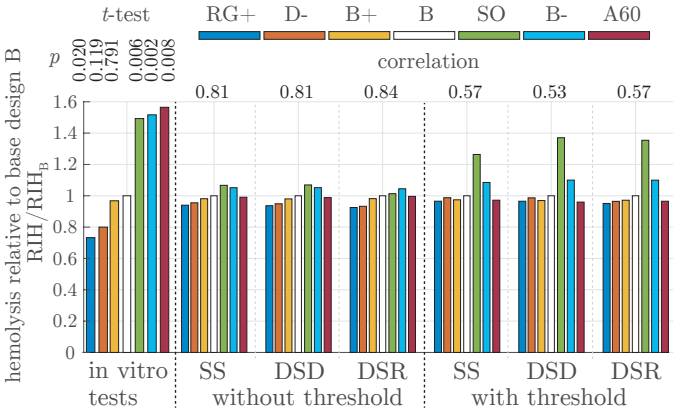

Fig. 6. Correlation between in vitro measurements and stationary CFD results.

Due to the good agreement in absolute hemolysis prediction and the highest correlation to in vitro experiments, the subsequent detailed examination of the cell damage is carried out with the DSR implementation. Due to the lower sensitivity and the sometimes different prediction trend, results of CFD simulations have to be interpreted with care.

VI. Results

A. Overview

The flow conditions are illustrated in Fig. 7 for the base design B. The fluid enters the impeller through the inlet eye and leaves the impeller blade at the trailing edge towards the volute. Within the volute, a strongly circulating flow is observed. The fluid finally exits the pump through the outlet nozzle. Furthermore, leakage flows pass through the shroud and hub clearance gap around the levitated impeller. At the nominal operating point, only 60% of the flow passing through the blades leaves the pump through the outlet nozzle. The remaining 40% are recirculating as leakage flow. They reduce the hydraulic efficiency of the pump but increase washouts in the gaps around the impeller, thus reducing residence time and cell destruction. Of the leakage flow, 60% recirculates through the shroud clearance gap to the blade impeller eye. The other 40% recirculates through the radial and hub clearance gap.

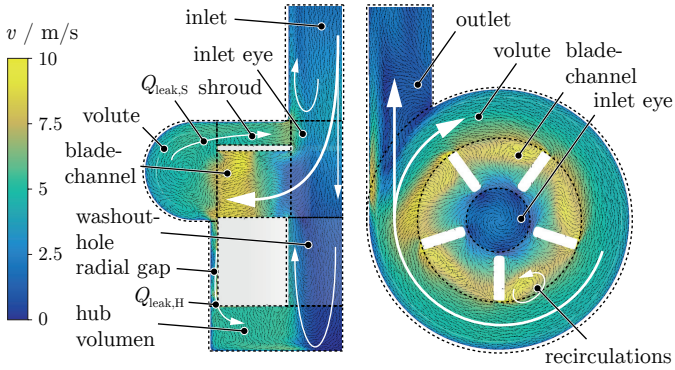

Fig. 7. Flow conditions and definitions of the side wall gaps.

Fig. 8 shows a cross-sectional top- and side-view of the hemolysis distribution in the base design pump B. Damaged blood is mainly located in the bottom volume underneath the impeller. In the center of the impeller, fresh, undamaged blood enters the pump and mixes with the hemolyzed blood.

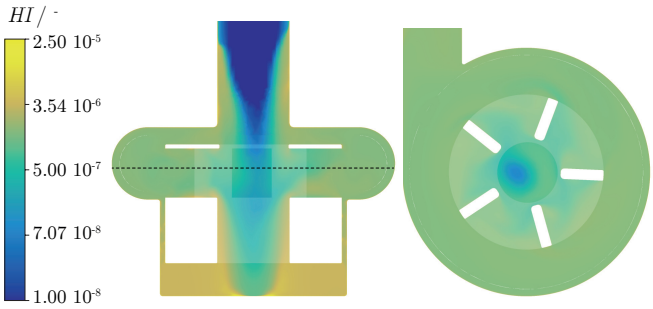

Fig. 8. Hemolysis distribution in the pump.

For the further analysis of the pump not the HI but the source term S_{HI} is of interest, as it describes the local cell destruction rates. It is illustrated in Fig. 9. The highest damage rate occurs in the boundary layer, near the impeller and housing walls. To make the distribution visible, a logarithmic scale is used.

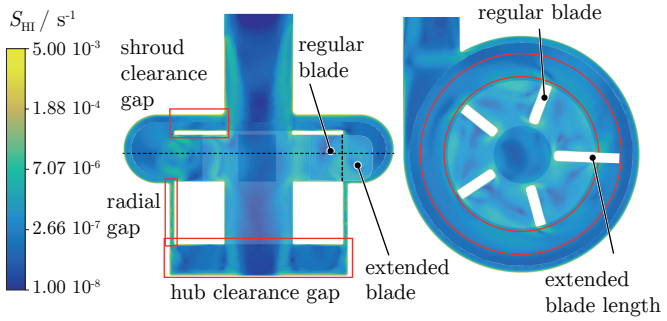

Fig. 9. Distribution of the source term S_{HI} within the base design shown with a logarithmic scale. The blade shape of impeller SO is illustrated exemplary at one of the impeller blades. Regions analyzed in more detail are indicated by red rectangles.

A summary of the damage source related to each of the individual regions defined in Fig. 7 is listed in Table VI. Due to its large volume and high shear stresses near the walls, the total source of hemolysis

$$\mathrm{HI}_{\mathrm{tot}} = \int_{\mathrm{V}} S_{\mathrm{HI,V}} \, \mathrm{d}V \tag{19}$$

is highest in the volute. Other regions with high total cell damage are the radial gap and the shroud and hub volumes. Especially the radial gap is of interest, since its damage density is by far the highest.

B. Critical Shear Stress Regions

Only 0.5% of the total priming volume (15.5 ml) is subject to overcritical shear stress $\tau > 150\,\mathrm{Pa}$. These regions are mainly located at the impeller and housing walls and are illustrated in Fig. 10. In addition, histogram plots of the shear distribution within the volume and at the housing and impeller walls are shown on the right hand side.

Considering the distribution of the shear stresses on the wall surface, highest stress occurs near the inlet nozzle fillet.

0018-9294 (c) 2020 IEEE. Personal use is permitted, but republication/redistribution requires IEEE permission. See http://www.ieee.org/publications_standards/publications/rights/index.html for more information.
Authorized licensed use limited to: ETH BIBLIOTHEK ZURICH. Downloaded on October 15,2020 at 12:50:59 UTC from IEEE Xplore. Restrictions apply.

This article has been accepted for publication in a future issue of this journal, but has not been fully edited. Content may change prior to final publication. Citation information: DOI 10.1109/TBME.2020.3030316, IEEE Transactions on Biomedical Engineering

TABLE VI
PORTIONS OF THE OVERALL CELL DAMAGE ATTRIBUTED TO INDIVIDUAL REGIONS WITHIN THE PUMP.

Region	Volume V cm^3	Total Source $\mathrm{HI}_{\mathrm{tot}}$ $\mathrm{m}^3/\mathrm{s} \cdot 10^{-12}$	Density $\mathrm{HI}_{\mathrm{tot}}/V$ $1/\mathrm{s} \cdot 10^{-6}$
Inlet	2.58	7.78	3.02
Outlet	2.51	5.71	2.27
Washout Hole	0.48	0.93	1.93
Inlet Eye	0.50	0.82	1.62
Radial Gap	0.37	28.17	76.76
Hub Volume	1.69	23.11	13.68
Blade Channel	1.55	8.35	5.39
Shroud Volume	0.65	18.59	28.69
Volute	4.65	44.25	9.51

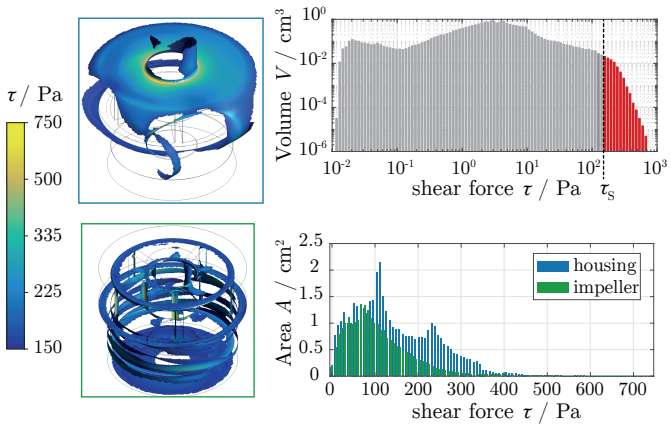

Fig. 10. Regions of overcritical shear stresses ($\boldsymbol{\tau > 150\,\mathrm{Pa}}$) and histograms of the shear force distribution within the volume and at the impeller and volute walls.

Values locally reach $780\,\mathrm{Pa}$. Most of the wall shear stress above $150\,\mathrm{Pa}$ is located on the housing wall.

C. Top Clearance Gap

Increasing the shroud clearance gap causes higher hemolysis. This was obtained by reducing the blade height (design B-) as well as by increasing the distance δ_{S} at constant blade height (design S+). Even though the shear stress in the shroud gap can be reduced slightly, the larger clearance causes a higher leakage flow $Q_{\mathrm{leak,S}}$. As a result, the volumetric efficiency of the impeller drops and higher rotational speeds are required. This causes more hemolysis in the side channels.

To improve the cell compatibility, the blade height can be increased (design B+), resulting in a higher volumetric efficiency and a lower nominal impeller speed. However, it must be ensured that the two boundary layers illustrated in Fig. 11 do not unify. This would cause increased shear forces and higher cell damage. The in vitro test results show that the achievable improvement is marginal (compare designs B and B+ in Table III)..

D. Bottom Clearance Gap

Below the impeller hub, cell damage is mainly caused at the housing bottom (see Fig. 12). Due to the low washout and large bottom volume, the residence time is long. To improve

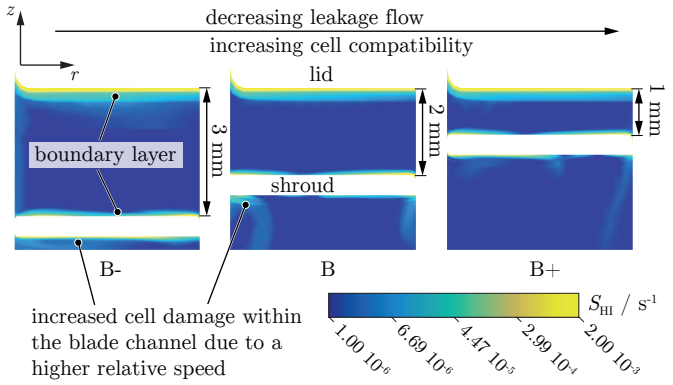

Fig. 11. Distribution of the source term $\boldsymbol{S_{\mathrm{HI}}}$ in the shroud clearance gap for variations B-, B, and B+ in logarithmic scale.

hemolysis, this volume can be reduced, which shortens the residence time. Similar to the top clearance gap, it must be ensured that the decreased distance δ_{H} does not lead to an unification of the boundary layers.

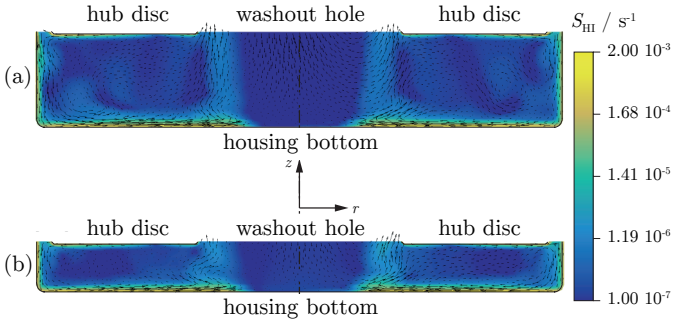

Fig. 12. Distribution of the source term $\boldsymbol{S_{\mathrm{HI}}}$ in the hub clearance gap for design variations B and H- in logarithmic scale.

E. Inlet Nozzle Fillet Radius

The high shear stress at the inlet nozzle causes high damage sources. Even though particles in this region reside only for a short time, significant cell damage is caused.

Increasing the fillet radius from $1\,\mathrm{mm}$ to $6\,\mathrm{mm}$ reduces the maximum source term from $6.6 \cdot 10^{-3}$ to $1.8 \cdot 10^{-3}$. Furthermore, the shear stress is distributed much better along the housing lid. This is due to the lower flow velocity resulting from the increased cross-sectional area.

Compared to the base design B, such an increased inlet fillet radius can reduce hemolysis by almost 40%.

F. Radial Gap

Within the narrow radial gap, between the impeller and housing, a Taylor-Couette flow regime evolves [52]. Several Taylor-vortices can be observed, originating near the impeller trailing edge and continuing around the circumference of the impeller towards the hub volume (see relative velocity w in Fig. 14(a)). Particles trapped within such vortices show longer residence times within the radial gap. Since the shear stress is high in this region, cell damage strongly accumulates for these particles while passing through the radial gap.

0018-9294 (c) 2020 IEEE. Personal use is permitted, but republication/redistribution requires IEEE permission. See http://www.ieee.org/publications_standards/publications/rights/index.html for more information.
Authorized licensed use limited to: ETH BIBLIOTHEK ZURICH. Downloaded on October 15,2020 at 12:50:59 UTC from IEEE Xplore. Restrictions apply.

This article has been accepted for publication in a future issue of this journal, but has not been fully edited. Content may change prior to final publication. Citation information: DOI 10.1109/TBME.2020.3030316, IEEE Transactions on Biomedical Engineering

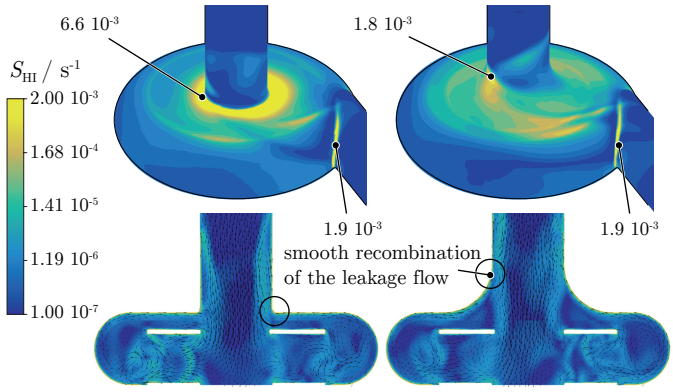

Fig. 13. Distribution on the source term S_{HI} on the housing walls for the variations B and R+. Logarithmic scale.

The vortices also cause higher relative velocities near the impeller and housing walls. Peak values are approximately six times higher compared to a stratified, vortex-less axial flow.

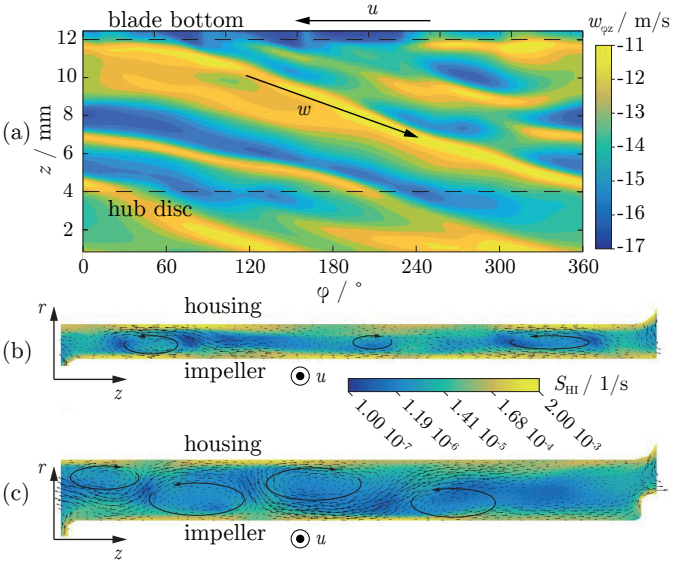

Fig. 14. Distribution of the source term S_{HI} in the radial clearance gap for variations B and RG+ in logarithmic scale.

By increasing the radial gap as illustrated in Fig. 14, Taylor-vortices become larger but the leakage flow $Q_{\mathrm{leak,H}}$ increases. As a result, the residence time reduces while the source terms remain almost unchanged. Cell destruction can be reduced by 25%.

G. Long Semi-Shrouded Blades

To reduce the circumferential speed of the impeller at the side walls, the blades can be extended towards the volute. This was implemented with the impeller design SO, as indicated in Fig. 9 and depicted in Fig. 1. The required rotational speed can be reduced from 7885 rpm to 5635 rpm. This reduces the shear stresses in all side gaps.

However, as the blades are reaching into the volute, high relative velocities occur between the blade extensions and the fluid (see Fig. 15 right). Specifically at $r = r_{\mathrm{a}}$, where the impeller shroud ends and the flow is decelerated.

Fig. 15 shows the S_{HI} distribution around the impeller blades within the volute. Especially close to the blade surface, the source term S_{HI} is increased. The induced vortices trailing the impeller blade introduce additional cell damage.

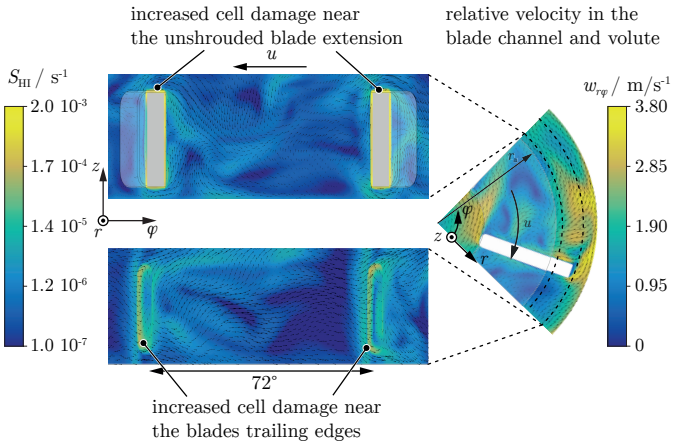

Fig. 15. Distribution of the source term S_{HI} in the volute for the variation SO. Logarithmic scale.

VII. Conclusions

For the presented bearingless centrifugal pumps, CFD assisted hemolysis prediction can be used to identify the major causes for hemolysis. The absolute error of the prediction depends on the parameter set, implementation method, and equivalent shear stress. Best agreement between in vitro experiments and CFD simulations were achieved with the parameter set of Fraser and equivalent shear stress $\tau_{\sqrt{3}}$. Predictions for the base design were within 10% when using a double-stage implementation with residence time as a first transport equation. The correlation between in vitro experiments and CFD results was 0.84 for the considered impeller variations.

Highest cell damage is caused in the radial gap, followed by the volute, shroud and hub regions. The use of a threshold shear stress did not result in better predictions.

Improvements regarding the cell compatibility can be achieved by increasing the radial gap and reducing the hub clearance gap δ_{H}. This causes the leakage flow to rise, resulting in a lower residence time within the high shear stress region. Further reduction in hemolysis is achieved by increasing the inlet nozzle fillet radius. This causes a smoother recombination of the leakage flow across the shroud gap $Q_{\mathrm{leak,S}}$ with the incoming flow and leads to a better distribution of the shear stress across the housing lid.

Except for the radial gap, clearance gaps should be kept small while ensuring sufficient distance, such that the boundary layers do not combine. Extending the blade length into the volute reduces the relative speed in the side wall volumes but introduces significant cell damage near the blade extension.

References

[1] T. V. Brogan, L. Lequier, R. Lorusso, G. MacLaren, and G. J. Peek, *Extracorporeal Life Support: The ELSO Red Book*. Extracorporeal Life Support Organization, 2017. [Online]. Available: https://www.elso.org/Publications/RedBook5thEdition.aspx

0018-9294 (c) 2020 IEEE. Personal use is permitted, but republication/redistribution requires IEEE permission. See http://www.ieee.org/publications_standards/publications/rights/index.html for more information.
Authorized licensed use limited to: ETH BIBLIOTHEK ZURICH. Downloaded on October 15,2020 at 12:50:59 UTC from IEEE Xplore. Restrictions apply.

This article has been accepted for publication in a future issue of this journal, but has not been fully edited. Content may change prior to final publication. Citation information: DOI 10.1109/TBME.2020.3030316, IEEE Transactions on Biomedical Engineering

[2] C. Betrus, R. Remenapp, J. Charpie, T. Kudelka, P. Brophy, W. E. Smoyer, and J. Lin, "Enhanced hemolysis in pediatric patients requiring extracorporeal membrane oxygenation and continuous renal replacement therapy," *Annals of Thoracic and Cardiovascular Surgery*, vol. 13, no. 6, p. 378, 2007.

[3] D. J. Schaer, P. W. Buehler, A. I. Alayash, J. D. Belcher, and G. M. Vercellotti, "Hemolysis and free hemoglobin revisited: exploring hemoglobin and hemin scavengers as a novel class of therapeutic proteins," *Blood*, vol. 121, no. 8, pp. 1276–1284, 02 2013. [Online]. Available: https://doi.org/10.1182/blood-2012-11-451229

[4] G. W. Burgreen, J. F. Antaki, Z. Wu, and A. J. Holmes, "Computational fluid dynamics as a development tool for rotary blood pumps," *Artificial Organs*, vol. 25, no. 5, pp. 336–340, 2001. [Online]. Available: https://onlinelibrary.wiley.com/doi/abs/10.1046/j.1525-1594.2001.025005336.x

[5] J. Apel, R. Paul, S. Klaus, T. Siess, and H. Reul, "Assessment of hemolysis related quantities in a microaxial blood pump by computational fluid dynamics," *Artificial Organs*, vol. 25, no. 5, pp. 341–347, 2001. [Online]. Available: https://onlinelibrary.wiley.com/doi/abs/10.1046/j.1525-1594.2001.025005341.x

[6] L. Wiegmann, S. Boës, D. de Zélicourt, B. Thamsen, M. S. Daners, M. Meboldt, and V. Kurtcuoglu, "Blood pump design variations and their influence on hydraulic performance and indicators of hemocompatibility," *Annals of Biomedical Engineering*, vol. 46, no. 3, pp. 417–428, 2018.

[7] H. Yu, S. Engel, G. Janiga, and D. Thévenin, "A review of hemolysis prediction models for computational fluid dynamics," *Artificial Organs*, 2017.

[8] M. E. Taskin, K. H. Fraser, T. Zhang, C. Wu, B. P. Griffith, and Z. J. Wu, "Evaluation of eulerian and lagrangian models for hemolysis estimation," *ASAIO Journal*, vol. 58, no. 4, pp. 363–372, 2012.

[9] M. Giersiepen, L. Wurzinger, R. Opitz, and H. Reul, "Estimation of shear stress-related blood damage in heart valve prostheses–in vitro comparison of 25 aortic valves." *The International Journal of Artificial Organs*, vol. 13, no. 5, pp. 300–306, 1990. [Online]. Available: http://www.ncbi.nlm.nih.gov/pubmed/2365485

[10] L. Wurzinger, R. Opitz, P. Blasberg, and H. Schmid-Schönbein, "Platelet and coagulation parameters following millisecond exposure to laminar shear stress." *Thrombosis and Haemostasis*, vol. 54, no. 2, pp. 381–386, 1985. [Online]. Available: http://www.ncbi.nlm.nih.gov/pubmed/2934855

[11] S. S. Lee, J. F. Antaki, M. V. Kameneva, J. G. Dobbe, M. R. Hardeman, K. H. Ahn, and S. J. Lee, "Strain hardening of red blood cells by accumulated cyclic supraphysiological stress," *Artificial Organs*, vol. 31, no. 1, pp. 80–86, 2007.

[12] L. Wurzinger, R. Opitz, and H. Eckstein, "Mechanical bloodtrauma. an overview," *Angeiologie*, vol. 38, no. 3, pp. 81–97, 1986.

[13] S. Hashimoto, "Erythrocyte destruction under periodically fluctuating shear rate: comparative study with constant shear rate," *Artificial Organs*, vol. 13, no. 5, pp. 458–463, 1989. [Online]. Available: http://www.ncbi.nlm.nih.gov/pubmed/2803057

[14] D. Steines, D. Westphal, C. Göbel, H. Reul, and G. Rau, "Platelet function and hemolysis in centrifugal pumps: In vitro investigations," *The International Journal of Artificial Organs*, vol. 22, no. 8, pp. 559–565, 1999, pMID: 10533912. [Online]. Available: https://doi.org/10.1177/039139889902200806

[15] C. Kramer, P. Sand, and W. Bleifeld, "Blutströmung und mechanische Hämolyse," *Biomedizinische Technik/Biomedical Engineering*, vol. 16, no. 5, pp. 164–168, 1971.

[16] G. Heuser and R. Opitz, "A couette viscometer for short time shearing of blood," *Biorheology*, vol. 17, no. 1-2, pp. 17–24, 1980.

[17] R. Indeglia, M. Shea, R. Forstrom, and E. Bernstein, "Influence of mechanical factors on erythrocyte sublethal damage," *ASAIO Journal*, vol. 14, no. 1, pp. 264–272, 1968.

[18] L. Leverett, J. Hellums, C. Alfrey, and E. Lynch, "Red blood cell damage by shear stress," *Biophysical Journal*, vol. 12, no. 3, pp. 257–273, mar 1972. [Online]. Available: http://dx.doi.org/10.1016/s0006-3495(72)86085-5

[19] R. Paul, J. Apel, S. Klaus, F. Schügner, P. Schwindke, and H. Reul, "Shear stress related blood damage in laminar couette flow," *Artificial Organs*, vol. 27, no. 6, pp. 517–529, Jun 2003. [Online]. Available: http://onlinelibrary.wiley.com/doi/10.1046/j.1525-1594.2003.07103.x/abstract

[20] A. M. Sallam and N. H. Hwang, "Human red blood cell hemolysis in a turbulent shear flow: contribution of reynolds shear stresses," *Biorheology*, vol. 21, no. 6, pp. 783–797, 1984.

[21] R. Eilers, "Einsatz und Bewertung rechnergestützter Methoden für die technische Auslegung mechanischer Herzklappenprothesen," Ph.D. dissertation, RWTH Aachen, 1997.

[22] L. Goubergrits and K. Affeld, "Numerical estimation of blood damage in artificial organs," *Artificial Organs*, vol. 28, no. 5, pp. 499–507, 2004.

[23] A. Garon and M.-I. Farinas, "Fast three-dimensional numerical hemolysis approximation," *Artificial Organs*, vol. 28, no. 11, pp. 1016–1025, 2004.

[24] A. Arvand, M. Hormes, and H. Reul, "A validated computational fluid dynamics model to estimate hemolysis in a rotary blood pump," *Artificial Organs*, vol. 29, no. 7, pp. 531–540, 2005.

[25] A. Mitoh, T. Yano, K. Sekine, Y. Mitamura, E. Okamoto, D.-W. Kim, R. Yozu, and S. Kawada, "Computational fluid dynamics analysis of an intra-cardiac axial flow pump," *Artificial Organs*, vol. 27, no. 1, pp. 34–40, 2003. [Online]. Available: https://onlinelibrary.wiley.com/doi/abs/10.1046/j.1525-1594.2003.07190.x

[26] T. Yano, K. Sekine, A. Mitoh, Y. Mitamura, E. Okamoto, D.-W. Kim, I. Nishimura, S. Murabayashi, and R. Yozu, "An estimation method of hemolysis within an axial flow blood pump by computational fluid dynamics analysis," *Artificial Organs*, vol. 27, no. 10, pp. 920–925, 2003. [Online]. Available: https://onlinelibrary.wiley.com/doi/abs/10.1046/j.1525-1594.2003.00034.x

[27] D. Lacasse, A. Garon, and D. Pelletier, "Mechanical hemolysis in blood flow: user-independent predictions with the solution of a partial differential equation," *Computer Methods in Biomechanics and Biomedical Engineering*, vol. 10, no. 1, pp. 1–12, 2007.

[28] M.-I. Farinas, A. Garon, D. Lacasse, and D. N'dri, "Asymptotically consistent numerical approximation of hemolysis," *Journal of Biomechanical Engineering*, vol. 128, no. 5, pp. 688–696, 2006.

[29] F. A. Salazar, J. F. Antaki *et al.*, "Numerical study of turbulence models in the computation of blood flow in cannulas," in *ASME 2008 Fluids Engineering Division Summer Meeting collocated with the Heat Transfer, Energy Sustainability, and 3rd Energy Nanotechnology Conferences*. American Society of Mechanical Engineers Digital Collection, 2009, pp. 999–1005.

[30] M. Grigioni, U. Morbiducci, G. D'Avenio, G. Di Benedetto, and C. Del Gaudio, "A novel formulation for blood trauma prediction by a modified power-law mathematical model," *Biomechanics and Modeling in Mechanobiology*, vol. 4, no. 4, pp. 249–260, 2005.

[31] H. Schima, M. R. Müller, S. Tsangaris, G. Gheiseder, C. Schlusche, U. Losert, H. Thoma, and E. Wolner, "Mechanical blood traumatization by tubing and throttles in in vitro pump tests: experimental results and implications for hemolysis theory," *Artificial Organs*, vol. 17, no. 3, pp. 164–170, 1993.

[32] M. E. Taskin, K. H. Fraser, T. Zhang, B. Gellman, A. Fleischli, K. A. Dasse, B. P. Griffith, and Z. J. Wu, "Computational characterization of flow and hemolytic performance of the ultramag blood pump for circulatory support," *Artificial Organs*, vol. 34, no. 12, pp. 1099–1113, dec 2010. [Online]. Available: http://dx.doi.org/10.1111/j.1525-1594.2010.01017.x

[33] H. Yu, "Flow design optimization of blood pumps considering hemolysis," Ph.D. dissertation, Magdeburg Universität, 2015. [Online]. Available: http://nbn-resolving.de/urn:nbn:de:gbv:ma9:1-6390

[34] B. Thamsen, B. Blümel, J. Schaller, C. O. Paschereit, K. Affeld, L. Goubergrits, and U. Kertzscher, "Numerical analysis of blood damage potential of the HeartMate II and Heartware HVAD rotary blood pumps," *Artificial Organs*, vol. 39, no. 8, pp. 651–659, 2015.

[35] X. Song, A. L. Throckmorton, H. G. Wood, J. F. Antaki, and D. B. Olsen, "Computational fluid dynamics prediction of blood damage in a centrifugal pump," *Artificial Organs*, vol. 27, no. 10, pp. 938–941, 2003. [Online]. Available: http://www.ncbi.nlm.nih.gov/pubmed/14616540

[36] T. Zhang, M. E. Taskin, H.-B. Fang, A. Pampori, R. Jarvik, B. P. Griffith, and Z. J. Wu, "Study of flow-induced hemolysis using novel couette-type blood-shearing devices," *Artificial Organs*, vol. 35, no. 12, pp. 1180–1186, aug 2011. [Online]. Available: http://dx.doi.org/10.1111/j.1525-1594.2011.01243.x

[37] K. H. Fraser, M. E. Taskin, B. P. Griffith, and Z. J. Wu, "The use of computational fluid dynamics in the development of ventricular assist devices," *Medical Engineering & Physics*, vol. 33, no. 3, pp. 263 – 280, 2011. [Online]. Available: http://www.sciencedirect.com/science/article/pii/S1350453310002456

[38] R. v. Mises, "Mechanik der festen Körper im plastisch-deformablen Zustand," *Nachrichten von der Gesellschaft der Wissenschaften zu Göttingen, Mathematisch-Physikalische Klasse*, vol. 1913, pp. 582–592, 1913.

0018-9294 (c) 2020 IEEE. Personal use is permitted, but republication/redistribution requires IEEE permission. See http://www.ieee.org/publications_standards/publications/rights/index.html for more information.
Authorized licensed use limited to: ETH BIBLIOTHEK ZURICH. Downloaded on October 15,2020 at 12:50:59 UTC from IEEE Xplore. Restrictions apply.

This article has been accepted for publication in a future issue of this journal, but has not been fully edited. Content may change prior to final publication. Citation information: DOI 10.1109/TBME.2020.3030316, IEEE Transactions on Biomedical Engineering

[39] M. M. Faghih and M. K. Sharp, "Modeling and prediction of flow-induced hemolysis: a review," *Biomechanics and Modeling in Mechanobiology*, vol. 18, no. 4, pp. 845–881, Aug 2019. [Online]. Available: https://doi.org/10.1007/s10237-019-01137-1

[40] M. M. Faghih and M. Keith Sharp, "Extending the power-law hemolysis model to complex flows," *Journal of Biomechanical Engineering*, vol. 138, no. 12, 11 2016. [Online]. Available: https://doi.org/10.1115/1.4034786

[41] C. Bludszuweit, "Three-dimensional numerical prediction of stress loading of blood particles in a centrifugal pump," *Artificial Organs*, vol. 19, no. 7, pp. 590–596, 1995.

[42] J. F. Gülich, *Centrifugal Pumps*. Springer, 2008, vol. 2.

[43] ASTM Committee and others, "Standard practice for assessment of hemolysis in continuous flow blood pumps," *Annual Book of ASTM Standards, F1844-97(2017)*, vol. 13, pp. 1–5, 2017.

[44] G. Moore, M. Ledford, and A. Merydith, "A micromodification of the drabkin hemoglobin assay for measuring plasma hemoglobin in the range of 5 to 2000 mg/dl," *Biochemical Medicine*, vol. 26, no. 2, pp. 167–173, 1981.

[45] K. Kawahito and Y. Nose, "Hemolysis in different centrifugal pumps," *Artificial Organs*, vol. 21, no. 4, pp. 323–326, 1997.

[46] K. Naito, E. Suenaga, Z.-L. Cao, H. Suda, T. Ueno, M. Natsuaki, and T. Itoh, "Comparative hemolysis study of clinically available centrifugal pumps," *Artificial Organs*, vol. 20, no. 5, pp. 560–563, 1996.

[47] F. Menter, "Zonal two equation kw turbulence models for aerodynamic flows," in *23rd Fluid Dynamics, Plasmadynamics, and Lasers Conference*, 1993, p. 2906.

[48] H. Schlichting and K. Gersten, *Grenzschichttheorie*. Springer-Verlag, 2006.

[49] S. Gross-Hardt, F. Boehning, U. Steinseifer, T. Schmitz-Rode, and T. A. S. Kaufmann, "Mesh sensitivity analysis for quantitative shear stress assessment in blood pumps using computational fluid dynamics," *Journal of Biomechanical Engineering*, vol. 141, no. 2, 12 2018, 021012. [Online]. Available: https://doi.org/10.1115/1.4042043

[50] Y. Alemu and D. Bluestein, "Flow-induced platelet activation and damage accumulation in a mechanical heart valve: numerical studies," *Artificial Organs*, vol. 31, no. 9, pp. 677–688, 2007.

[51] K. H. Fraser, T. Zhang, M. E. Taskin, B. P. Griffith, and Z. J. Wu, "A quantitative comparison of mechanical blood damage parameters in rotary ventricular assist devices: shear stress, exposure time and hemolysis index," *Journal of Biomechanical Engineering*, vol. 134, no. 8, p. 081002, 2012.

[52] G. I. Taylor, "Stability of a viscous liquid contained between two rotating cylinders," *Philosophical Transactions of the Royal Society of London. Series A, Containing Papers of a Mathematical or Physical Character*, vol. 223, no. 605-615, pp. 289–343, 1923.

0018-9294 (c) 2020 IEEE. Personal use is permitted, but republication/redistribution requires IEEE permission. See http://www.ieee.org/publications_standards/publications/rights/index.html for more information.
Authorized licensed use limited to: ETH BIBLIOTHEK ZURICH. Downloaded on October 15,2020 at 12:50:59 UTC from IEEE Xplore. Restrictions apply.